

MSFMamba: Multi-Scale Feature Fusion State Space Model for Multi-Source Remote Sensing Image Classification

Feng Gao, *Member, IEEE*, Xuepeng Jin, *Student Member, IEEE*, Xiaowei Zhou, Junyu Dong, *Member, IEEE*, Qian Du *Fellow, IEEE*

Abstract—In multi-source remote sensing image classification field, remarkable progress has been made by convolutional neural network and Transformer. However, existing methods are still limited due to the inherent local reductive bias. Recently, Mamba-based methods built upon the State Space Model have shown great potential for long-range dependency modeling with linear complexity, but it has rarely been explored for the multi-source remote sensing image classification task. To this end, we propose Multi-Scale Feature Fusion Mamba (MSFMamba) network for hyperspectral image (HSI) and LiDAR/SAR data joint classification. Specifically, MSFMamba mainly comprises three parts: Multi-Scale Spatial Mamba (MSpa-Mamba) block, Spectral Mamba (Spe-Mamba) block, and Fusion Mamba (Fus-Mamba) block. Specifically, to solve the feature redundancy in multiple canning routes, the MSpa-Mamba block incorporates the multi-scale strategy to minimize the computational redundancy and alleviate the feature redundancy of SSM. In addition, Spe-Mamba is designed for spectral feature exploration, which is essential for HSI feature modeling. Moreover, to alleviate the heterogeneous gap between HSI and LiDAR/SAR data, we design Fus-Mamba block for multi-source feature fusion. The original Mamba is extended to accommodate dual inputs, and cross-modal feature interaction is enhanced. Extensive experimental results on three multi-source remote sensing datasets demonstrate the superiority performance of the proposed MSFMamba over the state-of-the-art models. Source codes of MSFMamba will be made public available at <https://github.com/summitgao/MSFMamba>.

Index Terms—CNNs, Transformer models, Selective Structured State Space Model, Hyperspectral imaging, LiDAR/SAR data

I. INTRODUCTION

WITH the rapid development of remote sensing technology and sensor platforms, multi-source remote sensing data from various platforms such as satellites, aircraft, and drones have become increasingly abundant [1]. These data have been widely applied in land cover classification [2], geological resource exploration [3], urban planning [4], disaster warning [5], and agricultural monitoring [6]. Among these applications, land cover classification is an important and fundamental task [7] [8].

This work was supported in part by the National Science and Technology Major Project under Grant 2022ZD0117202, in part by the Natural Science Foundation of Qingdao under Grant 23-2-1-222-ZYYD-JCH, and in part by the Postdoctoral Fellowship Program of CPSF under Grant GZC20241614. (Corresponding author: Xiaowei Zhou.)

Feng Gao, Xuepeng Jin, Xiaowei Zhou, and Junyu Dong are with the School of Computer Science and Technology, Ocean University of China, Qingdao 266100, China.

Qian Du is with the Department of Electrical and Computer Engineering, Mississippi State University, Starkville, MS 39762 USA.

Among these multi-source data captured by various sensors, hyperspectral image (HSI), light detection and ranging (LiDAR) data, and synthetic aperture radar (SAR) data are of great significance. HSI can identify subtle differences among ground objects through its rich spectral information [9] [10] [11]. HSI classification has been widely studied, since the rich spectral information contained in HSI presents great opportunities and challenges. On the other hand, LiDAR data precisely measure the three-dimensional structure of terrain and objects with high spatial resolution and accuracy [12] [13]. SAR sensors perform imaging in all weather conditions and at all times, penetrating clouds and vegetation [14] [15] [16]. The fusion of HSI and LiDAR/SAR data can leverage the complementary advantages of both data sources and lead to improved ground object classification performance [17] [18] [19]. By combining the spectral information of HSI with the three-dimensional structural information of LiDAR or the all weather imaging capability of SAR, the limitations of a single data source can be alleviated and more reliable classification results can be achieved [20] [21]. Therefore, in this paper, we mainly focus on HSI and LiDAR/SAR data joint classification.

Because of diverse distributions and feature representations in multi-source images, the critical challenge for HSI and LiDAR/SAR data classification lies in how to bridge the heterogeneity gap. Recently, tremendous efforts have been made for multi-source data classification [22] [23]. The most common framework that demonstrated promising classification results employs CNN-based feature encoder in an end-to-end manner. Cross-guided attention [24], cross-channel correlation [25], federated learning [26] and cross-scale mixing attention [27] are employed for multi-source data classification. In addition, Transformer-based models have demonstrated outstanding long-range feature modeling capabilities in multi-source remote sensing data classification [28]. Spatial-spectral attention [29], hierarchical attention [30] [31], scale-adaptive attention [32] are used for HSI and LiDAR/SAR data classification.

Recently, an improved state-space model (SSM) [33] with a selective scanning mechanism, Mamba [34], has emerged as an effective alternative for computer vision and remote sensing image interpretation tasks. Compared with Transformer-based models, state-space sequence models reformulate the attention mechanism so that it scales linearly with the sequence length, and it significantly reduces the computational costs when the sequence is very long [35]. However, the SSM has rarely

been explored to solve the multi-source remote sensing image classification task.

It is a non-trivial and challenging task to introduce the SSM into multi-source data classification, due to the following reasons: 1) **Feature redundancy in multiple scanning routes.** To address the challenge of image data nondirectionality, existing SSM-based models generally use multi-scan strategy (Forward, backward, horizontal, and vertical scan) to ensure that every part of the image can establish connections with other parts. However, the multi-scan strategy significantly increases the feature redundancy. Therefore, how to reduce the information redundancy of SSM is one of the primary challenges we face. 2) **The Heterogeneous gap between multi-source data.** SSM's role in multi-source remote sensing data classification has not yet been fully explored, as SSM lacks a design similar to cross-attention. This prompts us to investigate how to use SSM to alleviate the heterogeneous gap between HSI and LiDAR/SAR data.

To address the above challenges, we propose **Multi-Scale Feature Fusion Mamba** (MSFMamba) network for the joint classification of HSI and LiDAR/SAR data. MSFMamba mainly comprises three parts: Multi-Scale Spatial Mamba (MSpa-Mamba) block, Spectral Mamba (Spe-Mamba) block, and Fusion Mamba (Fus-Mamba) block. Specifically, to solve the feature redundancy in multiple scanning routes, the MSpa-Mamba block incorporates the multi-scale strategy to minimize the computational redundancy and alleviate the feature redundancy in SSM. In addition, Spe-Mamba is designed for spectral feature exploration, which is essential for HSI feature modeling. Moreover, to alleviate the heterogeneous gap between HSI and LiDAR/SAR data, we design Fus-Mamba block for multi-source feature fusion. The original Mamba is extended to accommodate dual inputs, and cross-modal feature interaction is enhanced. Experimental results on three multi-source remote sensing datasets demonstrate the superior performance of the proposed MSFMamba.

In summary, our main contributions can be summarized as follows:

- Multi-Scale Spatial Mamba (MSpa-Mamba) block is designed to incorporate the multi-scale strategy to minimize the computational burden. To the best of our knowledge, this is the first work to investigate the multi-scale SSMs for multi-source remote sensing image classification.
- Fusion Mamba (Fus-Mamba) block is proposed to enhance cross-modal feature interactions between multi-source data.
- Extensive experiments on three public benchmark datasets reveal that our proposed method outperforms the state-of-the-art methods. As a side contribution, we will release our codes to benefit the other researchers interested in remote sensing image interpretation.

The remainder of this paper is organized as follows: Section II reviews related works. Section III introduces the preliminaries of the state space model and the detailed structure of MSFMamba. Experiments on three multi-source datasets are presented in Section IV. Conclusion and future works are drawn in Section V.

II. RELATED WORKS

A. Deep Learning-Based Multi-Source Image Classification

Deep learning-based multi-source data classification has witnessed significant progress recently. Convolutional neural networks (CNNs) have been widely used in an end-to-end manner for multi-source feature fusion. Dong et al. [24] used self-attention and cross-guided attention to emphasize interesting regions and channels of multi-source features. Gao et al. [27] presented a cross-mixing attention network to extract multi-scale features for hyperspectral and multispectral image joint classification. Xu et al. [36] introduced a dual-tunnel CNN architecture that separately extracts spectral-spatial features from HSI and LiDAR data. Zhang et al. [37] proposed a model known as patch-to-patch CNN for multi-source data classification. They constructed a three-tower structure to compute multi-scale features. Mohla et al. [38] proposed FusAtNet, which leverages HSI to generate an attention map via self-attention mechanism, which effectively highlights the intrinsic spectral features. In addition, cross-attention is employed to fuse the multi-source features. Fang et al. [39] presented the spatial-spectral enhancement module to promote multi-modal feature interaction.

To enhance the long-range feature dependencies, many Transformer-based methods have been proposed for multi-source remote sensing image classification. Hu et al. [40] proposed a simple yet effective parallel Transformer model. One Transformer acts as HSI feature encoder, and the other one is responsible for cross-modal feature interactions. Zhao et al. [41] proposed a CNN and Transformer hybrid model for HSI and LiDAR data classification. Cross-token attention is used for cross-modal feature fusion. Yao et al. [42] proposed Extended Vision Transformer (ExViT), which modifies the traditional ViT to handle land use and land cover classification tasks. This framework processes multimodal remote sensing image data through parallel branches and introduces a cross-modality attention module to enhance information exchange between different modalities. Li et al. [43] introduced mixing attention and convolution network for multi-source feature fusion. Although these CNN and Transformer-based methods have gained performance improvement, there is still an urgent need for an efficient and effective scheme to model the heterogeneous representation. In this paper, we explore Mamba's potential for multi-source remote sensing feature fusion, providing an effective paradigm to propel the progress of heterogeneous feature fusion.

B. State Space Model

State-Space Models (SSM) [33] [44] [45] have become practical components for constructing deep networks due to their cutting-edge performance in analyzing continuous long sequential data. Gu et al. [45] introduced a diagonal structure and combined it with a diagonal plus low-rank approach to construct structured SSM. Smith et al. [33] improved the efficiency of SSM by introducing parallel scanning techniques. Mamba [34] incorporates data-dependent parameters to amend the linear time invariant characteristics of SSM-based models,

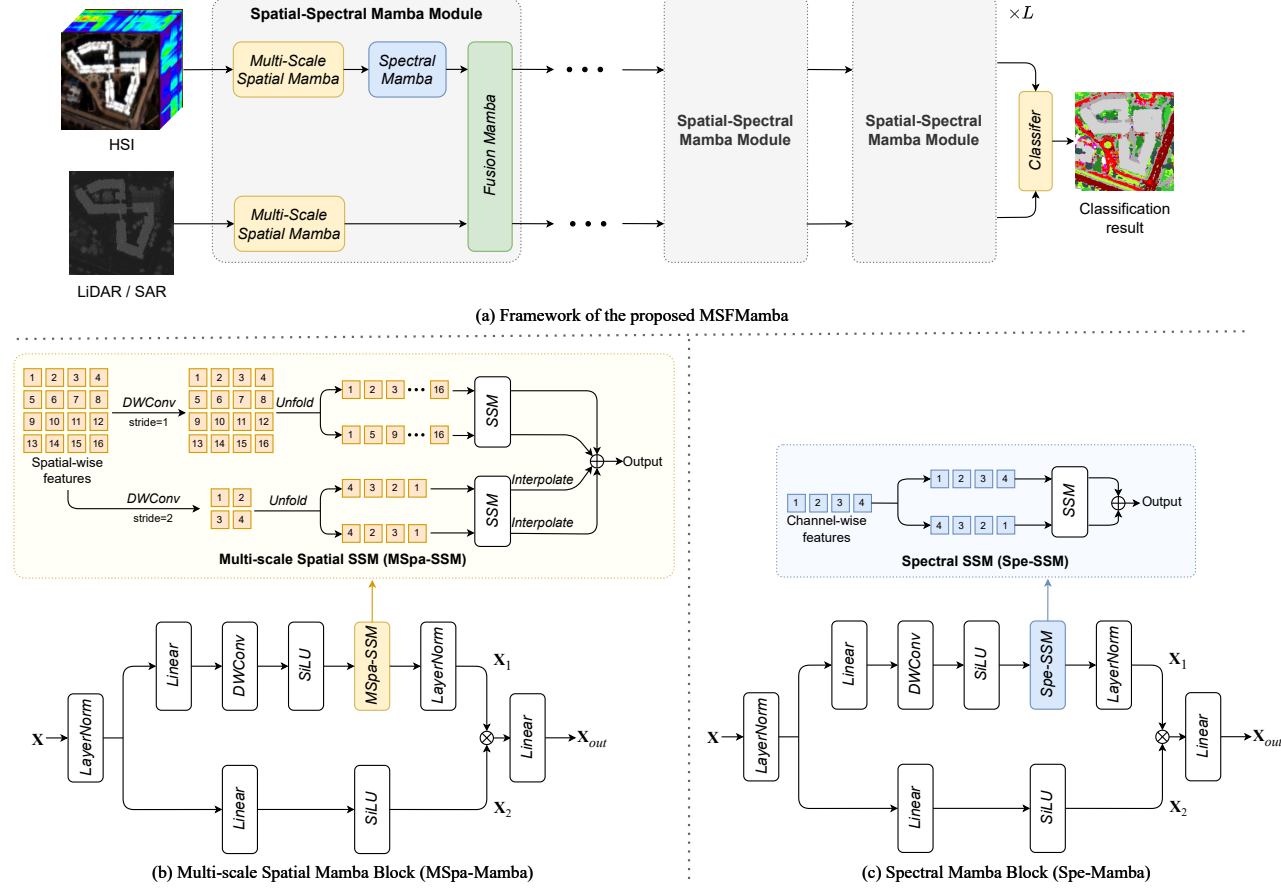


Fig. 1. Framework of the proposed Multi-Scale Feature Fusion Mamba (MSFMamba) for HSI and LiDAR/SAR data classification. (a) Details of the proposed MSFMamba. It contains L spatial-spectral Mamba module to learn multi-source feature representations. Each spatial-spectral Mamba module is comprised of Multi-scale Spatial Mamba (MSpa-Mamba) block, Spectral Mamba (Spe-Mamba) block, and Fusion Mamba (Fus-Mamba) block. (b) Details of the MSpa-Mamba block, as well as the Multi-scale Spatial SSM (MSpa-SSM). (c) Details of the Spe-Mamba block, as well as the Spectral SSM (Spe-SSM).

and it has demonstrated excellent performance over Transformers on large-scale datasets.

Recently, inspired by pioneering SSMs, Mamba-like frameworks have been employed in computer vision and remote sensing image interpretation tasks, such as VMamba [46], RS³Mamba [47], and RSMamba [48]. RSMamba [48] employed dynamic multi-path activation mechanism to enhance the performance of remote sensing image classification. Zhang et al. [49] employed a unique encoder architecture, based on the Mamba design, to effectively extract semantic information from remote sensing images. Chen et al. [50] used a Mamba-like feature encoder to learn global spatial contextual information for remote sensing image change detection. Li et al. [51] proposed a spectral Mamba block to extract the spectral features of HSI, and improve the HSI classification performance. These works show the potential for extension into multi-source data fusion, its particular application in HSI and LiDAR/SAR data joint classification tasks remains unexplored.

III. METHODOLOGY

In this section, we start by presenting the essential concepts of the state space model. Following that, we delve into a

comprehensive description of our MSFMamba, covering its framework and module design in detail.

A. Preliminaries

State-Space Model (SSM). SSM is a linear time-invariant system that map an input sequence $x(t) \in \mathbb{R}^N$ to an output sequence $y(t) \in \mathbb{R}^N$. They are mathematically represented by linear ordinary differential equations:

$$h'(t) = \mathbf{A}h(t) + \mathbf{B}x(t), \quad (1)$$

$$y(t) = \mathbf{C}h(t) + \mathbf{D}x(t), \quad (2)$$

where $h(t) \in \mathbb{R}^N$ indicate hidden state. $h'(t) \in \mathbb{R}^N$ refers to the time derivative of $h(t)$. N represents the number of states. Additionally, $\mathbf{A} \in \mathbb{R}^{N \times N}$ is the state transition matrix. $\mathbf{B} \in \mathbb{R}^{N \times 1}$ and $\mathbf{C} \in \mathbb{R}^{N \times 1}$ are projection matrices. $\mathbf{D} \in \mathbb{R}^{N \times 1}$ is served as a residual connected operation.

SSMs are continuous-time models, and pose challenges when incorporated into deep learning networks. To solve the problem, discrete versions of SSMs are proposed, and the ordinary differential equations can be discretized by the zeroth-order hold rule. A timescale parameter Δ is incorporated

to convert the continuous parameters \mathbf{A} , \mathbf{B} into discrete parameters $\overline{\mathbf{A}}$, $\overline{\mathbf{B}}$ as follows:

$$\overline{\mathbf{A}} = \exp(\Delta \mathbf{A}), \quad (3)$$

$$\overline{\mathbf{B}} = (\Delta \mathbf{A})^{-1}(\exp(\Delta \mathbf{A}) - \mathbf{I}) \cdot \Delta \mathbf{B}. \quad (4)$$

The projection matrix $\overline{\mathbf{B}}$ can be approximated using the first-order Taylor series. After discretization, the ordinary differential equations of SSMs can be represented as follows:

$$\begin{aligned} h_t &= \overline{\mathbf{A}} h_{t-1} + \overline{\mathbf{B}} x_t \\ y_t &= \mathbf{C} h_t + \mathbf{D} x_t \end{aligned} \quad (5)$$

Selective Scan Mechanism. Traditional SSMs use a linear time-invariant framework, which means that the projection matrices remain fixed and unaffected by variations in the input sequence. However, this static configuration results in a lack of attention on individual elements within the sequence. To alleviate this limitation, Mamba [34] proposes a solution where the parameter matrices become input-dependent. In this way, SSMs can better manage complex sequences, potentially enhancing their capability through the transformation into linear time-varying systems.

B. Overall Framework of the Proposed MSFMamba

As depicted in Fig. 1, our MSFMamba consists of two parts: 1) The main network with a series of L spatial-spectral Mamba modules to learn high-quality multi-source feature representations. 2) A classifier composed of two fully-connected layers for land cover classification. The number of spatial-spectral Mamba module L is a critical parameter that will be discussed in the experiments.

The HSI is first handled by Principal Component Analysis (PCA) to select the best N_p spectral bands. The HSI and LiDAR/SAR data are fed into the spatial-spectral Mamba modules for feature extraction and cross-modal feature fusion. The spatial-spectral Mamba modules are repeated L times, and the final features are concatenated and fed into the classifier for classification. The classifier consists of two fully-connected layers.

The Spatial-Spectral Mamba Module is the critical component in our MSFMamba. Details of the Spatial-Spectral Mamba Module are illustrated in Fig. 1(a). The input HSI and LiDAR/SAR features are first fed into the Multi-Scale Spatial Mamba (MSpa-Mamba) block for spatial feature extraction. To further exploit the spectral features of HSI, the Spectral Mamba (Spe-Mamba) block is employed for HSI feature extraction. Then, we obtain optimized features \mathbf{F}_h and \mathbf{F}_x . Next, \mathbf{F}_h and \mathbf{F}_x are fed into the Fusion Mamba block for cross-modal feature fusion and refinement. Finally, the refined HSI feature \mathbf{F}'_h and LiDAR/SAR feature \mathbf{F}'_x are generated.

As can be observed from Fig. 1(a), the MSSpa-Mamba block, Spe-Mamba block, and Fusion Mamba block are three key components in the Spatial-Spectral Mamba Module. We will give detailed descriptions of the three blocks in the following subsections.

C. Multi-Scale Spatial Mamba Block (MSpa-Mamba)

Overview of the MSpa-Mamba. The Mamba can model long-range feature dependencies, which is critical for understanding the global context in remote sensing images. Existing SSM-based models commonly use multi-scan strategy to ensure that every part of the image can establish connections with other parts. However, the multi-scale strategy significantly increases the feature redundancy of SSM.

To solve the problem, we design a simple yet effective Multi-scale Spatial Mamba (MSpa-Mamba) block. As shown in Fig. 1(b), the input feature $\mathbf{X} \in \mathbb{R}^{H \times W \times C}$ is fed into two parallel branches. In the first branch, the feature is processed by a linear layer, followed by a depth-wise convolution (DWConv), SiLU activation function, together with the Multi-scale Spatial SSM (MSpa-SSM) layer and LayerNorm. In the second branch, the feature is processed by a linear layer followed by the SiLU activation function. After that, features from the two branches are aggregated with element-wise multiplication. The computation of MSpa-Mamba block is as follows:

$$\mathbf{X}_1 = \text{LN}(\text{MSpa-SSM}(\text{SiLU}(\text{DWConv}(\text{Linear}(\mathbf{X})))), \quad (6)$$

$$\mathbf{X}_2 = \text{SiLU}(\text{Linear}((\mathbf{X}))), \quad (7)$$

$$\mathbf{X}_{out} = \text{Linear}(\mathbf{X}_1 \odot \mathbf{X}_2), \quad (8)$$

where LN denotes the LayerNorm, and \odot denotes the element-wise multiplication.

Multi-Scale Spatial SSM (MSpa-SSM). As shown in Fig. 1(b), MSpa-SSM is the critical part of the MSpa-Mamba block. In MSpa-SSM, features at multiple scales are generated through depth-wise convolution (DWConv) with different stride values. These multi-scale feature maps are then handled by four scanning routes within SSM [46]. The scanning routes are divided into two groups: Two maintain the original resolution and are processed by the SSM. The others are downsampled, processed by the SSM, and then upsampled. To be more specific, we use DWConv with strides of 1 and 2 to obtain feature map $\mathbf{Z}_1 \in \mathbb{R}^{H \times W \times C}$ and $\mathbf{Z}_2 \in \mathbb{R}^{\frac{H}{2} \times \frac{W}{2} \times C}$, respectively. Next, \mathbf{Z}_1 and \mathbf{Z}_2 are fed into the SSM as follows:

$$[\mathbf{Y}_1, \mathbf{Y}_2] = \text{SSM}(\sigma_1(\mathbf{Z}_1), \sigma_1(\mathbf{Z}_2)), \quad (9)$$

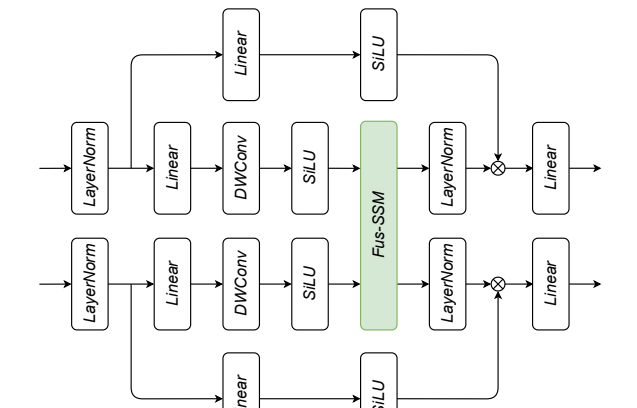
$$[\mathbf{Y}_3, \mathbf{Y}_4] = \text{SSM}(\sigma_3(\mathbf{Z}_3), \sigma_4(\mathbf{Z}_4)), \quad (10)$$

where σ is the transformation that converts 2D feature maps into 1D sequences in SSM. \mathbf{Y} is the processed sequence. The obtained sequences are converted back into 2D feature maps, and the downsampled feature maps are interpolated for merging as follows:

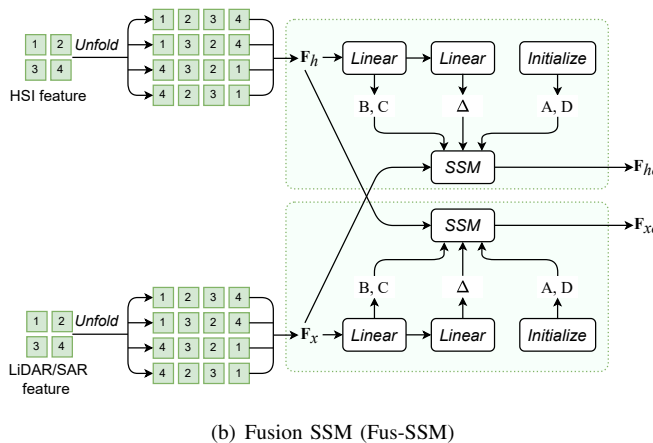
$$\mathbf{Z}'_i = \beta_i(\mathbf{Y}_i), \quad i \in \{1, 2, 3, 4\}, \quad (11)$$

$$\mathbf{Z}' = \mathbf{Z}'_1 + \mathbf{Z}'_2 + \text{Inter}(\mathbf{Z}'_3 + \mathbf{Z}'_4), \quad (12)$$

where β is the inverse transformation of σ . \mathbf{Z}' is the feature map enhanced by SSM. 'Inter' represents the interpolation operation.



(a) Fusion Mamba (Fus-Mamba) block



(b) Fusion SSM (Fus-SSM)

Fig. 2. Illustration of Fusion Mamba (Fus-Mamba) block, as well as the Fusion SSM (Fus-SSM).

D. Spectral Mamba Block (Spe-Mamba)

HSI covers a much larger spectral range and higher spectral resolution. How to model the relationship between spectra is an important problem. In this paper, we design a Spectral Mamba (Spe-Mamba) block for spectral feature modeling.

Details of the Spe-Mamba are illustrated in Fig. 1(c). The input feature is fed into two parallel branches. In the first branch, the feature is handled by a linear layer, DWConv, and SiLU activation, together with the Spectral SSM (Spe-SSM) layer. In the second branch, the feature is handled by a linear layer and SiLU activation. Finally, features from both branches are aggregated with element-wise multiplication.

It should be noted that the Spe-Mamba has similar structures with the MSpa-Mamba. The difference between Spe-Mamba and MSpa-Mamba is the SSM layer. In MSpa-SSM, the features are converted into 1D sequences along the spatial dimension. While in Spe-Mamba, the features are converted into 1D sequences along the channel dimension, and the features are only scanned in two directions.

E. Fusion Mamba Block (Fus-Mamba)

Traditional SSMs only handle single inputs, and they hardly combine the cross-modal information from multi-source data.

Algorithm 1 The computation of \mathbf{F}_{ho} in Fig. 2(b)

Input: $\mathbf{F}_h, \mathbf{F}_x : (P, C), (P, C)$

Output: $\mathbf{F}_{ho} : (P, C)$

- 1: $\mathbf{A} : (C, N) \leftarrow \text{Parameter}$
- 2: $\mathbf{D} : (C) \leftarrow \text{Parameter}$
/* A and D are randomly initialized. */
- 3: $\mathbf{B} : (P, N) \leftarrow \text{Linear}(\mathbf{F}_h)$
- 4: $\mathbf{C} : (P, N) \leftarrow \text{Linear}(\mathbf{F}_h)$
- 5: $\Delta : (P, C) \leftarrow \log(1 + \exp(\text{Linear}(\mathbf{F}_h) + \text{Parameter}))$
/* The selection mechanism */
- 6: $\overline{\mathbf{A}} : (P, C, N) \leftarrow \exp(\Delta \otimes \mathbf{A})$
- 7: $\overline{\mathbf{B}} : (P, C, N) \leftarrow \Delta \otimes \mathbf{B}$
- 8: $\mathbf{F}_{ho} \leftarrow \text{SSM}(\overline{\mathbf{A}}, \overline{\mathbf{B}}, \mathbf{C}, \mathbf{D})(\mathbf{F}_x)$
/* SSM denotes Eq. 5 implemented by selective scan */

return \mathbf{F}_{ho}

To solve the problem, we propose Fusion Mamba (Fus-Mamba) block to integrate features from different modalities. As shown in Fig. 2, the HSI and LiDAR/SAR features undergo the same processing procedure, which is similar to the MSpa-Mamba and Spe-Mamba. Multi-source features are fed into the Fusion-SSM (Fus-SSM) block for cross-modal feature fusion and interaction.

The Fus-SSM is the critical part of Fus-Mamba, and details of the Fus-SSM are illustrated in Fig. 2(b). Fus-SSM has a symmetric structure. On the top part, sequenced HSI feature $\mathbf{F}_h \in \mathbb{R}^{P \times C}$ is responsible for generating the projection and timescale parameters, while the sequenced LiDAR/SAR feature $\mathbf{F}_x \in \mathbb{R}^{P \times C}$ is to be handled to generate the output feature \mathbf{F}_{ho} . The bottom part of Fus-SSM has a similar structure with the top part. \mathbf{F}_x is responsible for generating the projection and timescale parameters, while \mathbf{F}_h is to be processed to generate the output feature \mathbf{F}_{xo} .

Algorithm 1 shows the detailed computation process of \mathbf{F}_{ho} . A and D are initialized at the beginning, while B, C, and Δ are obtained through linear layers from the input sequence \mathbf{F}_h . In the original Mamba, the sequence fed into SSM is input sequence \mathbf{F}_h , while in the proposed Fus-SSM, the sequence fed into SSM is from another modality \mathbf{F}_x . Since the computation of \mathbf{F}_{xo} is very similar to that of \mathbf{F}_{ho} , detailed description will not be repeated here.

IV. EXPERIMENTAL RESULTS AND ANALYSIS

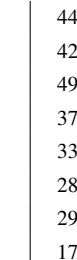
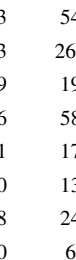
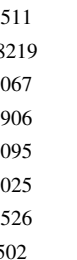
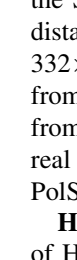
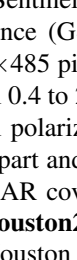
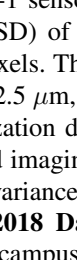
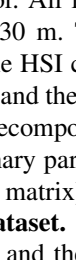
A. Dataset Description

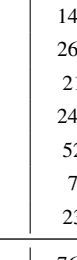
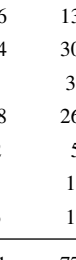
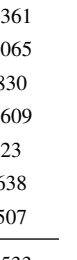
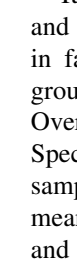
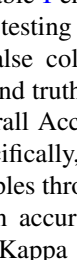
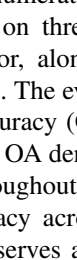
To assess the effectiveness of our proposed MSFMamba, we employ it to three multi-source remote sensing datasets: Berlin, Augsburg, and Houston 2018. The Berlin and Augsburg datasets are utilized for hyperspectral and SAR data classification, while the Houston 2018 dataset is employed for hyperspectral and LiDAR data classification.

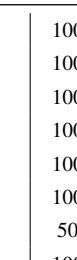
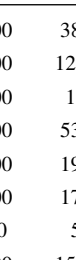
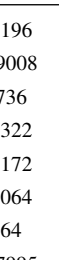
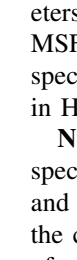
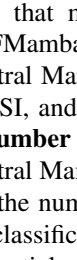
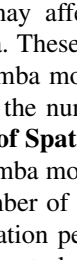
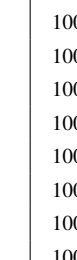
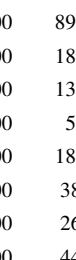
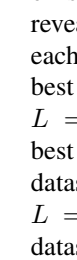
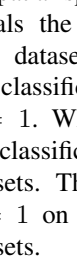
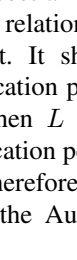
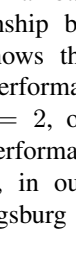
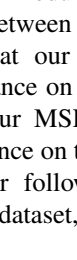
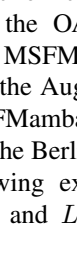
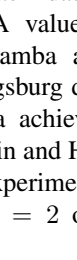
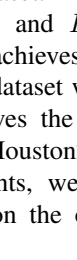
Berlin Dataset. It covers the urban and rural areas of Berlin. The hyperspectral data is simulated EnMAP data based on HyMap data. The SAR data is Sentinel-1 dual-Pol (VV–VH) single look complex (SLC) product obtained from the European Space Agency (ESA) [52]. The HSI has 797×220 pixels, 244 spectral bands in the wavelength range

TABLE I

THE NUMBER OF TRAINING AND TEST SAMPLES FOR THE BERLIN, AUGSBURG, AND HOUSTON2018 DATASETS.

Berlin dataset				
No.	Name	Color	Train	Test
1	Forest		443	54511
2	Residential area		423	268219
3	Industrial area		499	19067
4	Low plants		376	58906
5	Soil		331	17095
6	Allotment		280	13025
7	Commercial area		298	24526
8	Water		170	6502
Total			2820	461851

Augsburg dataset				
No.	Name	Color	Train	Test
1	Forest		146	13361
2	Residential area		264	30065
3	Industrial area		21	3830
4	Low plants		248	26609
5	Allotment		52	523
6	Commercial area		7	1638
7	Water		23	1507
Total			761	77533

Houston2018 dataset				
No.	Name	Color	Train	Test
1	Health grass		1000	38196
2	Stressed grass		1000	129008
3	Artificial turf		1000	1736
4	Evergreen trees		1000	53322
5	Deciduous trees		1000	19172
6	Bare earth		1000	17064
7	Water		500	564
8	Residential buildings		1000	157995
9	Non-residential buildings		1000	893769
10	Roads		1000	182283
11	Sidewalks		1000	135035
12	Crosswalks		1000	5059
13	Major thoroughfares		1000	184438
14	Highways		1000	38438
15	Railways		1000	26748
16	Paved parking lots		1000	44932
17	Unpaved parking lots		250	337
18	Cars		1000	25289
19	Trains		1000	20479
20	Stadium seats		1000	26296
Total			18750	2000160

of 400–2500 nm [53]. The SAR image has 1723×476 pixels. The nearest neighbor interpolation was employed to match the spatial resolution of the HSI and SAR data.

Augsburg Dataset. This dataset is composed of HSI and SAR data from Augsburg, Germany. The HSI was acquired by the HySpex sensor, and the SAR data was acquired by the Sentinel-1 sensor. All images are with the ground sample distance (GSD) of 30 m. The spatial size of both images is 332×485 pixels. The HSI contains 180 spectral bands ranging from 0.4 to $2.5 \mu\text{m}$, and the SAR data has four features derived from polarization decomposition (VV intensity, VH intensity, real part and imaginary part of the off-diagonal element of the PolSAR covariance matrix).

Houston2018 Dataset. This dataset covers the University of Houston campus and the neighboring urban area. The HSI contains 48 bands in the wavelength range of 380–1050 nm. LiDAR data is a multispectral LiDAR data with three bands. The University of Houston released the dataset as part of the 2018 IEEE GRSS Data Fusion Contest [54]. We use the training subset of the whole dataset in this paper.

Table I enumerates the number of samples for both training and testing on three datasets. Fig. 3 displays the HSI data in false color, along with the LiDAR/SAR images and the ground truth. The evaluation metrics used in this paper include Overall Accuracy (OA), Average Accuracy (AA), and Kappa. Specifically, OA denotes the proportion of accurately classified samples throughout the entirety of the dataset, AA signifies the mean accuracy across all classes present within the dataset, and Kappa serves as a statistical measure of the concurrence between predicted and true labels.

B. Parameter Analysis

We provide a detailed analysis of several important parameters that may affect the classification performance of our MSFMamba. These parameters include the number of spatial-spectral Mamba module, the number of principal components in HSI, and the number of state in SSM.

Number of Spatial-Spectral Mamba Module. The spatial-spectral Mamba module is the critical part in our MSFMamba, and the number of the module L is a key parameter affecting the classification performance. We tested the optimal number of spatial-spectral Mamba module on each dataset. Fig. 4 reveals the relationship between the OA value and L on each dataset. It shows that our MSFMamba achieves the best classification performance on the Augsburg dataset when $L = 1$. When $L = 2$, our MSFMamba achieves the best classification performance on the Berlin and Houston2018 datasets. Therefore, in our following experiments, we use $L = 1$ on the Augsburg dataset, and $L = 2$ on the other datasets.

Number of Principal Components in HSI. We use PCA to reduce the spectral redundancy of the input HSI. The number of principal components N_p is a critical parameter. We test different values of N_p ranging from 20 to 40, and the experimental results are shown in Fig. 5. It can be seen that when $N_p = 30$, the OA values for Augsburg and Houston2018 achieve the best, and when $N_p = 35$, the OA value for Berlin achieves the best.

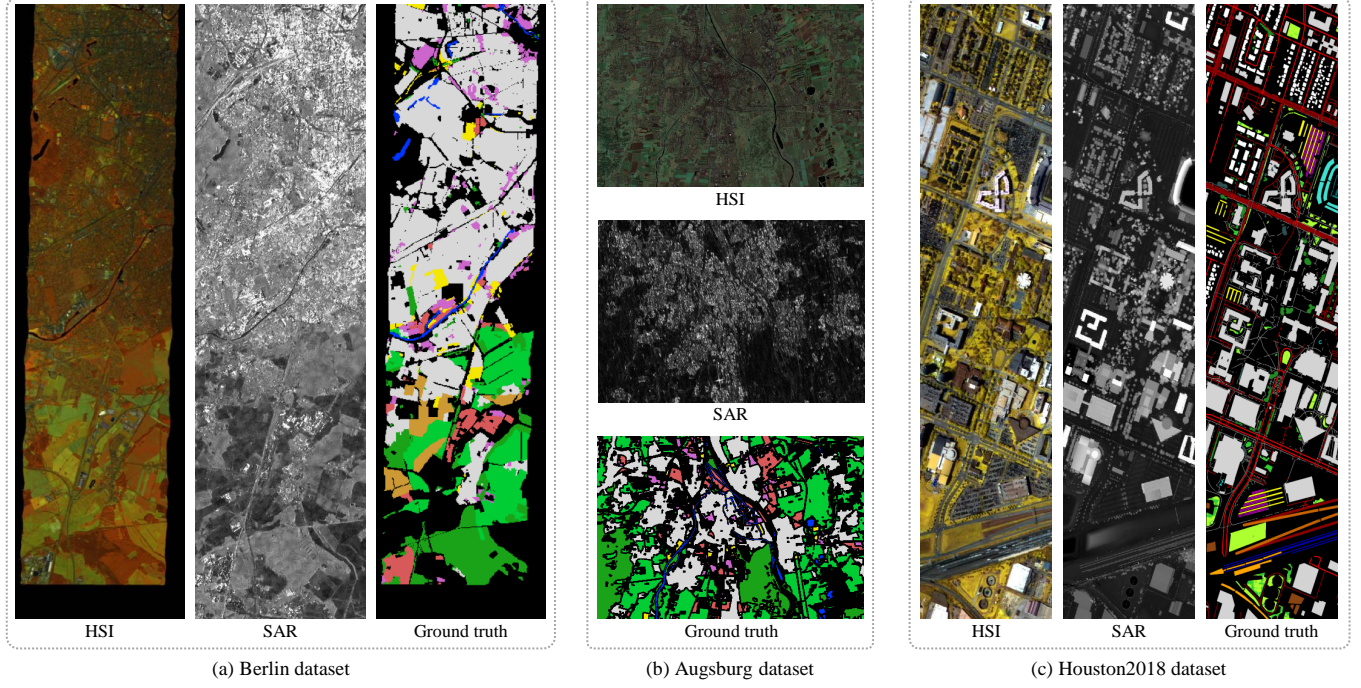


Fig. 3. Visualization of the three datasets used in our experiments. (a) Berlin dataset. (b) Augsburg dataset. (c) Houston 2018 dataset.

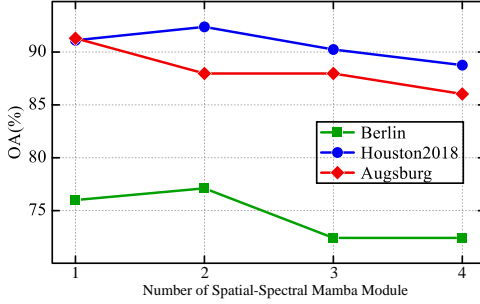


Fig. 4. The relationship between OA and the number of spatial-spectral Mamba module.

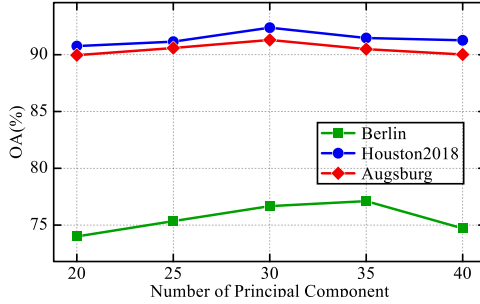


Fig. 5. The relationship between OA and the number of principal components in HSI.

Number of States in SSM. The number of states is an important parameter in the state space model. We tested five different number of states ranging from 4 to 20. As shown in Fig. 6, the optimal number of states for the Houston2018 and Berlin datasets is 16, while for the Augsburg dataset, the optimal number of states is 8.

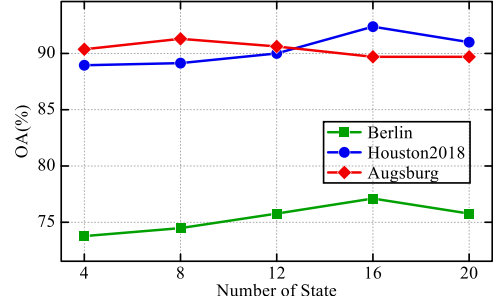


Fig. 6. The relationship between OA and the number of states in SSM.

The best settings of these experiments were used to evaluate our MSFMamba for comparison with the other state-of-the-art methods. All experiments were performed with an RTX 4090 GPU and 32GB of RAM using PyTorch.

C. Performance Comparison

We compare the proposed MSFMamba with existing state-of-the-art methods, including TBCNN [36], FusAtNet [38], S^2 ENet [39], DFINet [55], AsyFFNet [56], ExViT [42], HCT [41] and MACN [43]. TBCNN [36] investigates the classification fusion of hyperspectral imagery and data from other sensors using a two-branch convolution neural network. FusAtNet [38] presents a multi-source classification framework by utilizing a self-attention mechanism for spectral features and a cross-attention approach for spatial features. S^2 ENet [39] proposes a spatial-spectral enhancement module for cross-modal information interaction, which effectively facilitates the feature interaction between multi-source data. DFINet [55] uses a depth-wise cross attention module to extract complementary

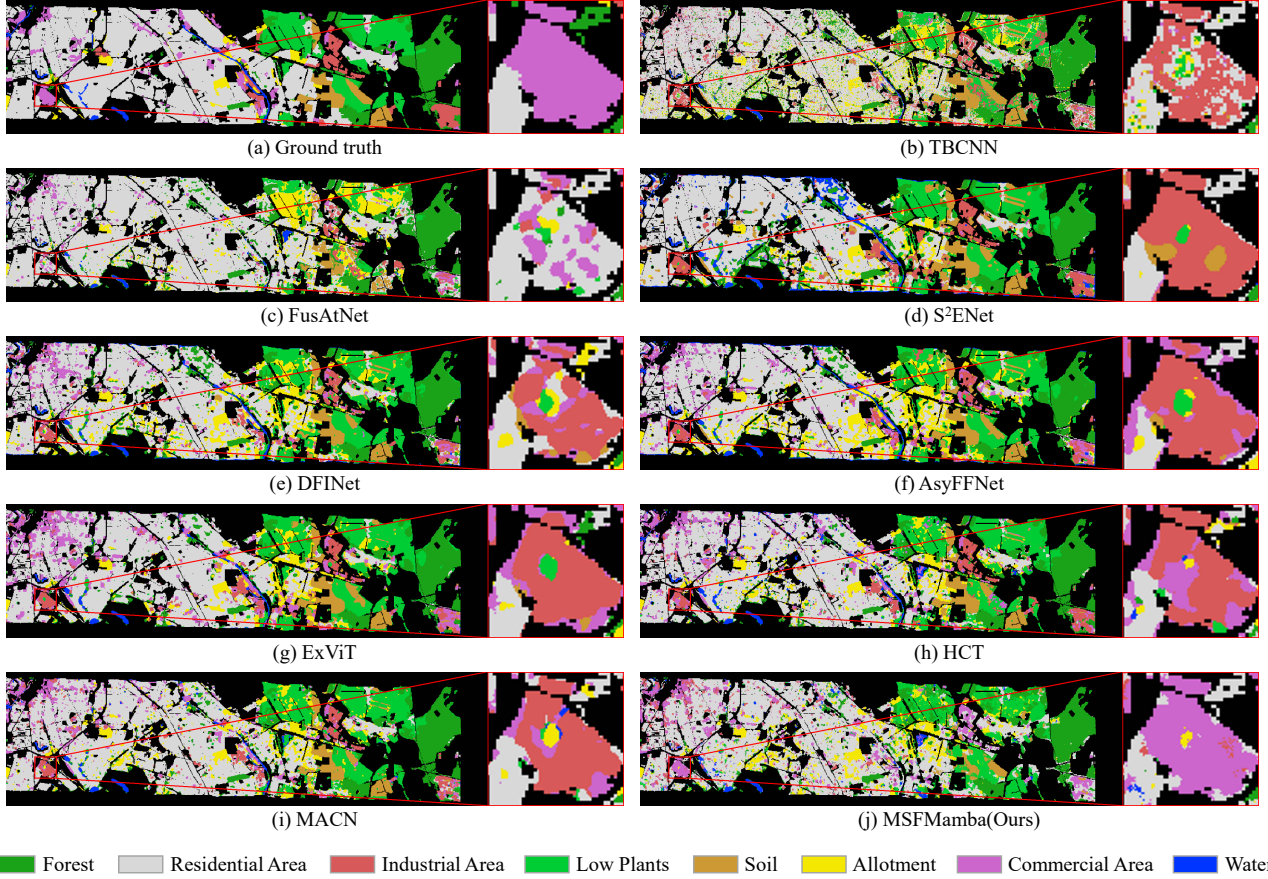


Fig. 7. Classification results of different methods for the Berlin dataset. (a) Ground Truth. (b) TBCNN. (c) FusAtNet. (d) S^2 ENet. (e) DFINet. (f) AsyFFNet. (g) ExViT. (h) HCT. (i) MACN. (j) proposed MSFMamba.

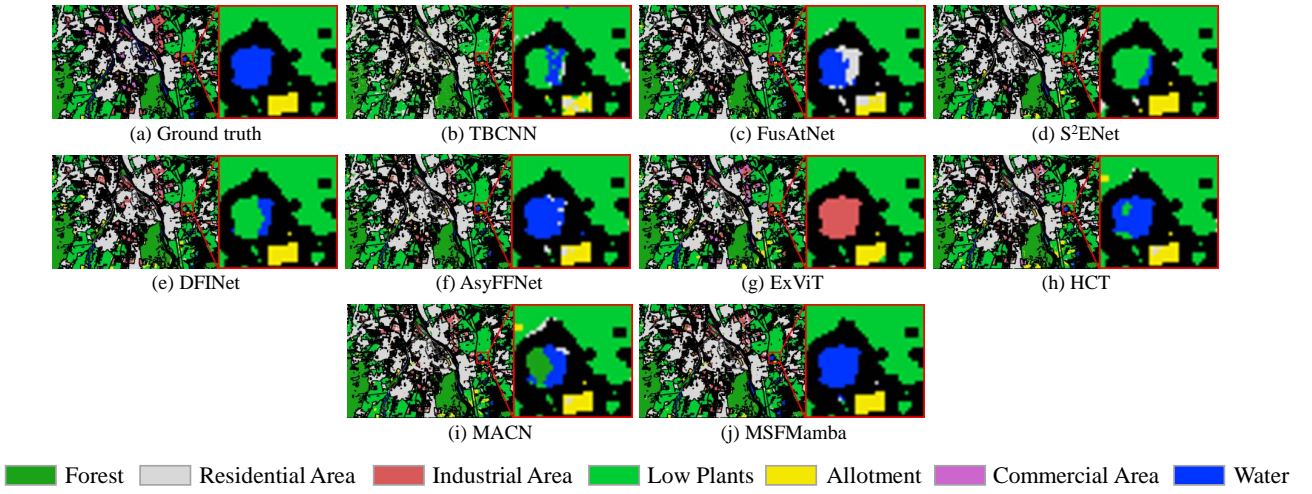


Fig. 8. Classification results of different methods for the Augsburg dataset. (a) Ground Truth. (b) TBCNN. (c) FusAtNet. (d) S^2 ENet. (e) DFINet. (f) AsyFFNet. (g) ExViT. (h) HCT. (i) MACN. (j) Proposed MSFMamba.

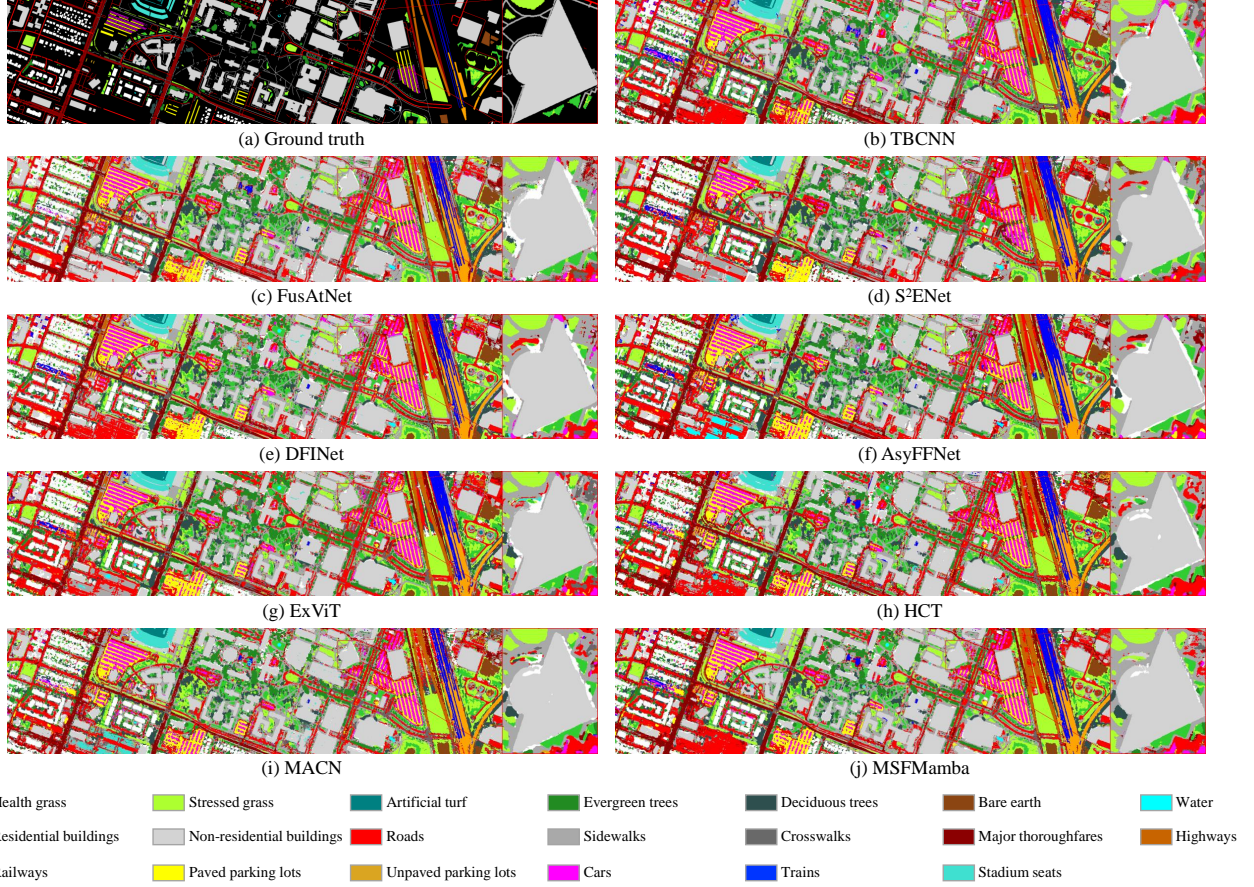


Fig. 9. Classification results of different methods for the Houston 2018 dataset. (a) Ground Truth. (b) TBCNN. (c) FusAtNet. (d) S^2 ENet. (e) DFINet. (f) AsyFFNet. (g) ExViT. (h) HCT. (i) MACN. (j) Proposed MSFMamba.

TABLE II
CLASSIFICATION PERFORMANCE OF DIFFERENT METHODS ON THE BERLIN DATASET.

Class	TBCNN	FusAtNet	S^2 ENet	DFINet	AsyFFNet	ExViT	HCT	MACN	MSFMamba
Forest	79.51	86.24	76.22	76.90	81.02	62.71	78.56	77.44	81.05
Residential area	92.27	91.38	95.09	93.41	93.62	94.34	93.71	92.73	93.00
Industrial area	42.27	19.76	41.84	37.09	38.90	41.02	44.48	41.38	47.96
Low plants	72.10	20.00	68.53	62.76	71.52	68.79	72.79	74.56	75.81
Soil	65.05	48.72	60.19	66.99	71.08	60.62	74.73	77.29	79.16
Allotment	17.59	38.89	42.56	46.15	26.04	26.71	28.21	24.44	38.35
Commercial area	15.49	18.47	16.42	18.80	13.23	35.01	26.28	25.04	33.37
Water	66.37	29.61	68.00	66.94	66.43	62.14	43.78	57.49	30.83
OA	67.92	70.91	71.26	73.73	73.04	73.89	75.51	74.42	77.11
AA	62.84	44.13	67.69	63.50	67.32	63.56	67.78	65.96	67.93
Kappa	54.32	51.07	59.08	61.02	60.76	61.62	63.70	62.11	65.57

information from multisource feature pairs. AsyFFNet [56] is a multi-source data classification method based on asymmetric feature fusion, which employs weight-share residual blocks for feature extraction and a feature calibration module for the spatial-wise multi-source feature modeling. ExViT [42] utilizes parallel branches of position-shared Transformer extended with separable convolution modules to process multi-modal image patches. In MACN [43], mixing self-attention and convolution Transformer layer is proposed to extract local and global multi-scale feature perception.

1) *Results on the Berlin Dataset.* The classification perfor-

mance of different methods on the Berlin dataset are shown in Table II. The corresponding classification maps are shown in Fig. 7. The proposed MSFMamba achieves the best OA of 77.11% and the best Kappa of 65.57%. It is evident that the proposed MSFMamba has strong multi-scale spatial contextual modeling capability from the sequence modeling perspective. From the visualized results, it is evident that the classification map generated by our MSFMamba is closer to the ground truth and more accurately in the details of local textures.

2) *Results on the Augsburg Dataset.* Table III illustrates the quantitative results of different methods on the Augsburg

TABLE III
CLASSIFICATION PERFORMANCE OF DIFFERENT METHODS ON THE AUGSBURG DATASET.

Class	TBCNN	FusAtNet	S^2 ENet	DFINet	AsyFFNet	ExViT	HCT	MACN	MSFMamba
Forest	90.88	93.78	97.06	97.38	97.47	90.04	97.07	96.52	97.55
Residential area	93.89	97.58	88.05	98.37	90.19	95.44	90.95	91.96	89.63
Industrial area	8.28	26.48	70.77	61.31	56.09	34.58	60.07	60.98	60.87
Low plants	91.97	97.67	96.88	92.63	97.38	90.68	95.57	96.64	97.94
Allotment	38.24	52.77	41.58	49.33	21.10	51.82	15.92	23.02	25.31
Commercial area	1.40	24.66	24.24	3.54	11.31	28.63	10.95	11.44	7.14
Water	10.82	47.51	81.82	26.61	87.59	17.65	84.64	83.92	88.09
OA	84.53	90.62	91.14	90.66	90.44	86.65	89.91	90.83	91.30
AA	47.92	62.92	62.51	61.30	62.91	58.40	61.27	62.36	64.42
Kappa	77.13	86.33	87.06	86.47	86.17	80.79	85.39	86.74	87.39

TABLE IV
CLASSIFICATION PERFORMANCE OF DIFFERENT METHODS ON THE HOUSTON 2018 DATASET.

Class	TBCNN	FusAtNet	S^2 ENet	DFINet	AsyFFNet	ExViT	HCT	MACN	MSFMamba
Health grass	87.25	86.20	71.85	75.46	94.87	84.55	74.15	86.24	83.78
Stressed grass	96.62	93.34	99.25	95.39	93.89	89.13	96.94	93.91	94.56
Artificial turf	93.99	93.38	96.55	97.04	85.01	94.30	96.18	92.13	97.97
Evergreen trees	88.95	92.34	96.10	90.67	86.89	94.36	90.22	91.23	90.48
Deciduous trees	67.68	73.69	95.42	79.39	69.24	70.15	78.61	74.07	79.53
Bare earth	85.83	96.60	99.47	98.51	93.08	71.79	95.94	98.68	98.33
Water	98.26	99.12	61.57	93.07	98.43	90.82	97.92	66.74	95.27
Residential buildings	72.83	81.23	82.24	80.47	90.84	80.92	89.35	84.54	85.76
Non-residential buildings	99.71	99.29	99.56	99.72	99.39	99.68	99.14	99.42	99.47
Roads	76.15	85.40	82.39	89.61	85.87	88.06	82.86	85.43	89.96
Sidewalks	73.35	78.06	81.08	76.19	79.24	75.48	83.45	73.86	79.42
Crosswalks	7.70	22.68	13.56	22.99	18.02	19.58	19.36	14.49	26.85
Major thoroughfares	84.03	79.88	77.67	86.89	84.11	84.19	86.22	86.10	86.80
Highways	80.15	79.11	76.00	80.47	92.84	80.80	80.09	80.91	80.96
Railways	97.34	96.55	98.75	98.00	93.70	95.21	97.29	97.82	98.69
Paved parking lots	90.50	92.07	96.17	94.03	85.61	94.78	93.60	91.79	91.25
Unpaved parking lots	90.84	62.29	78.55	97.68	47.13	85.75	55.89	96.47	98.83
Cars	83.87	85.67	91.39	89.83	82.38	87.53	87.03	88.31	93.75
Trains	91.71	87.75	94.09	94.68	82.92	94.99	90.53	96.37	94.79
Stadium seats	91.69	95.76	95.48	76.02	98.36	86.86	97.63	89.51	99.58
OA	86.75	90.25	90.05	90.84	91.41	90.17	91.62	90.42	92.38
AA	92.70	94.25	93.13	95.34	93.67	94.17	95.10	94.69	95.51
Kappa	83.10	87.43	87.19	88.25	88.90	87.39	89.15	87.68	90.16

TABLE V
INFLUENCE OF MSpA-MAMBA, SPE-MAMBA AND FUS-MAMBA ON CLASSIFICATION RESULTS OF MSFMAMBA.

MSpa-Mamba	Spe-Mamba	Fus-Mamba		Berlin	Augsburg	Houston2018
✓	✗	✗		74.88	89.05	89.56
✓	✓	✗		76.00	90.60	91.44
✓	✗	✓		75.88	90.55	91.76
✓	✓	✓		77.11	91.30	92.38

dataset. The corresponding classification maps of different methods are shown in Fig. 8. Benefiting from extraction of spatial-spectral semantic features with the sequential modeling mechanism, the proposed MSFMamba exhibits the most clear boundaries, fewer misclassified regions. From Table III, it can be observed that our MSFMamba improves upon the second-best algorithm by 0.16% in OA, 1.91% in AA, and 0.33% in Kappa. The excellent performance improvements by our MSFMamba verifies the effectiveness of sequential scanning model for multi-source data classification.

3) *Results on the Houston2018 Dataset.* Table IV illustrates

the quantitative results of various models on the Houston2018 dataset. Fig. 9 shows the corresponding classification maps of different methods. The proposed MSFMamba produces a well-defined classification map, in which the most noise regions are removed. From the visualized classification results in Fig. 9, the proposed MSFMamba is observed to be the closest to the ground truth, with fewer misclassified regions. The experimental results demonstrate that sequential scanning model is especially effective for HSI and LiDAR data joint classification.

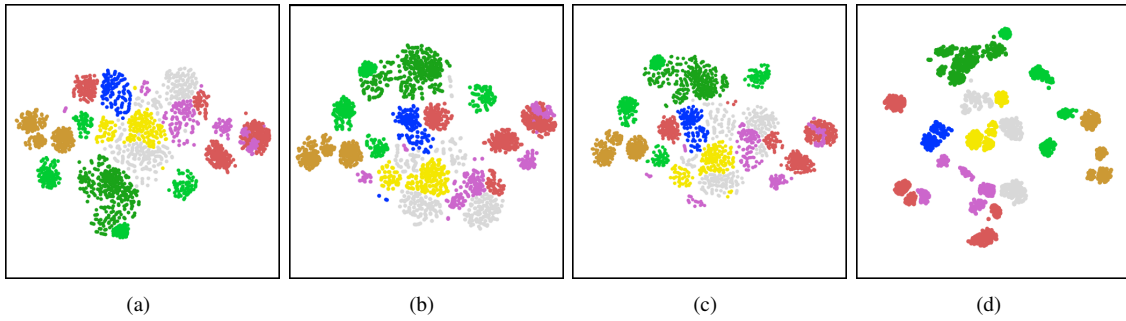


Fig. 10. t-SNE visualization of MSFMamba with different components. (a) MSpa-Mamba. (b) MSpa-Mamba + Spe-Mamba. (c) MSpa-Mamba + Fus-Mamba. (d) Full model of our MSFMamba.

TABLE VI
COMPARATIVE ANALYSIS OF MODEL PARAMETERS AND FLOPS ON THE AUGSBURG DATASET

Metrics	FusAtNet	S^2 ENet	DFINet	AsyFFNet	ExVit	HCT	MACN	MSFMamba
Params (M)	37.7177	1.4701	1.3155	2.4132	1.8848	4.7811	2.0199	1.5252
FLOPS (G)	3.5619	0.1779	0.1191	0.2064	0.2901	0.0437	0.1672	0.0377

D. Ablation Study

To evaluate the effectiveness of the key components of our proposed MSFMamba model, we conducted ablation studies on three datasets. These studies aim to explore the impacts of MSpa-Mamba, Spe-Mamba, and Fus-Mamba. Table VI shows the effects of different modules on the classification results. The results indicate that using MSpa-Mamba as a fundamental module achieves 74.88%, 89.05%, and 89.56% for OA on three datasets, respectively. The inclusion of Spe-Mamba further enhances the classification accuracies to 76.00%, 90.60%, and 91.44%. This demonstrates that Spe-Mamba plays a crucial role in classification, highlighting the importance of spectral information for joint classification of HSI and SAR/LiDAR data. Using MSpa-Mamba and Fus-Mamba achieves classification accuracies of 75.88%, 90.55%, and 91.76%, respectively. This indicates that better fusion of multi-source data is crucial for classification tasks. Finally, the combination of all three components achieves the best performance on three datasets. It demonstrates that the MSpa-Mamba, Spe-Mamba, and Fus-Mamba all contributes to the enhancement of classification accuracy.

We conducted t-SNE visualizations of the three components on the Berlin dataset for our MSFMamba, and the results are illustrated in Fig. 10. It can be observed that with only MSpa-Mamba, the features of different classes are less compact. With all the three modules, the feature representations display the most distinct, well-defined clusters compared with the others. It is evident that sequential scanning model generate more robust feature representations for multi-source data classification.

E. Analysis of Computational Complexity

We investigate the computational complexity of the proposed MSFMamba, with an emphasis on model parameters and FLOPs. Table VI provides the detailed model parameters and FLOPs of different methods on the Augsburg dataset. As

can be observed that the proposed MSFMamba requires fewer parameters than most of the existing methods. The FLOPs of our MSFMamba is the lowest, which indicate that our model has an advantage in computational efficiency. It is beneficial for deploying and running the proposed MSFMamba on edge devices such as drones and mobile devices.

V. CONCLUSIONS AND FUTURE WORK

In this paper, we present a novel MSFMamba network to tackle the multi-source remote sensing data joint classification task. SSM-based blocks are designed to leverage the advantages of linear complexity and large receptive field. Specifically, we design MSpa-Mamba block for spatial feature extraction. The multi-scale strategy is incorporated to minimize the computational redundancy and alleviate feature redundancy of SSM. In addition, Spe-Mamba block is incorporated for spectral feature extraction from the hyperspectral data, which is essential for HSI and LiDAR/SAR data fusion. Moreover, we design Fus-Mamba block for multi-source feature fusion. The original Mamba is extended to accommodate dual inputs, and cross-modal feature interaction is enhanced. The proposed MSFMamba achieves state-of-the-art performance on three multi-source remote sensing datasets, highlighting the effectiveness of MSFMamba.

In the future, we will explicitly explore the hybrid framework of Mamba and Transformer to further improve the long-range feature modeling capacity. Moreover, for a more comprehensive multi-source remote sensing data interpretation, it may be necessary to study the interpretability of the Mamba model for multi-source remote sensing data applications.

REFERENCES

- [1] M. Zhang, W. Li, and Q. Du, “Collaborative classification of hyperspectral and visible images with convolutional neural network,” *Journal of Applied Remote Sensing*, vol. 11, pp. 1–12, 09 2017.
- [2] J. Yue, L. Fang, and M. He, “Spectral-spatial latent reconstruction for open-set hyperspectral image classification,” *IEEE Transactions on Image Processing*, vol. 31, pp. 5227–5241, 2022.

- [3] H. Shirmand, E. Farahbakhsh, R. D. Müller, and R. Chandra, "A review of machine learning in processing remote sensing data for mineral exploration," *Remote Sensing of Environment*, vol. 268, pp. 1–21, 2022.
- [4] C. Wang, L. Zhang, W. Wei, and Y. Zhang, "Dynamic super-pixel normalization for robust hyperspectral image classification," *IEEE Transactions on Geoscience and Remote Sensing*, vol. 61, pp. 1–13, 2023.
- [5] N. Jiang, H.-B. Li, C.-J. Li, H.-X. Xiao, and J.-W. Zhou, "A fusion method using terrestrial laser scanning and unmanned aerial vehicle photogrammetry for landslide deformation monitoring under complex terrain conditions," *IEEE Transactions on Geoscience and Remote Sensing*, vol. 60, pp. 1–14, 2022.
- [6] S. Khanal, K. Kc, J. P. Fulton, S. Shearer, and E. Ozkan, "Remote sensing in agriculture—accomplishments, limitations, and opportunities," *Remote Sensing*, vol. 12, no. 22, p. 3783, 2020.
- [7] Z. Huang, J. Cheng, G. Wei, X. Hua, and Y. Wang, "An urban land cover classification method based on segments' multidimension feature fusion," *IEEE Journal of Selected Topics in Applied Earth Observations and Remote Sensing*, vol. 17, pp. 5580–5593, 2024.
- [8] K. Karantzalos, D. Bliziotis, and A. Karmas, "A scalable geospatial web service for near real-time, high-resolution land cover mapping," *IEEE Journal of Selected Topics in Applied Earth Observations and Remote Sensing*, vol. 8, no. 10, pp. 4665–4674, 2015.
- [9] Z. Li, K. Zheng, J. Li, C. Li, and L. Gao, "Cross-semantic heterogeneous modeling network for hyperspectral image classification," *IEEE Transactions on Geoscience and Remote Sensing*, vol. 62, pp. 1–16, 2024.
- [10] X. Zhao, M. Song, and T. Yang, "Hyperspectral unmixing based on chaotic sequence optimization of lp norm," *IEEE Geoscience and Remote Sensing Letters*, vol. 21, pp. 1–5, 2024.
- [11] D. Hong, W. He, N. Yokoya, J. Yao, L. Gao, L. Zhang, J. Chanussot, and X. Zhu, "Interpretable hyperspectral artificial intelligence: When non-convex modeling meets hyperspectral remote sensing," *IEEE Geoscience and Remote Sensing Magazine*, vol. 9, no. 2, pp. 52–87, 2021.
- [12] P. W. Milonni, "Lidar: range-resolved optical remote sensing of the atmosphere, in the springer series in optical sciences, vol. 102, edited by claus weitkamp: Scope: review. level: specialist," 2009.
- [13] M. Pashaei, M. J. Starek, and J. Berryhill, "Full-waveform terrestrial lidar data classification using raw digitized waveform signals," in *IEEE International Geoscience and Remote Sensing Symposium (IGARSS)*, 2022, pp. 1916–1919.
- [14] J. Shi and H. Jin, "Riemannian nearest-regularized subspace classification for polarimetric sar images," *IEEE Geoscience and Remote Sensing Letters*, vol. 19, pp. 1–5, 2022.
- [15] J. Cheng, D. Xiang, Q. Yin, and F. Zhang, "A novel crop classification method based on the tensor-gcn for time-series polsar data," *IEEE Transactions on Geoscience and Remote Sensing*, vol. 60, pp. 1–14, 2022.
- [16] J. Ni, C. López-Martínez, Z. Hu, and F. Zhang, "Multitemporal sar and polarimetric sar optimization and classification: Reinterpreting temporal coherence," *IEEE Transactions on Geoscience and Remote Sensing*, vol. 60, pp. 1–17, 2022.
- [17] J. X. Yang, J. Zhou, J. Wang, H. Tian, and A. W.-C. Liew, "Lidar-guided cross-attention fusion for hyperspectral band selection and image classification," *IEEE Transactions on Geoscience and Remote Sensing*, vol. 62, pp. 1–15, 2024.
- [18] X. Meng, S. Zhang, Q. Liu, G. Yang, and W. Sun, "Uncertain category-aware fusion network for hyperspectral and lidar joint classification," *IEEE Transactions on Geoscience and Remote Sensing*, vol. 62, pp. 1–15, 2024.
- [19] Y. Gao, W. Li, J. Wang, M. Zhang, and R. Tao, "Relationship learning from multisource images via spatial-spectral perception network," *IEEE Transactions on Image Processing*, vol. 33, pp. 3271–3284, 2024.
- [20] M. Zheng and Y. Zhang, "Dem-aided bundle adjustment with multi-source satellite imagery: Zy-3 and gf-1 in large areas," *IEEE Geoscience and Remote Sensing Letters*, vol. 13, no. 6, pp. 880–884, 2016.
- [21] Z. Xu, J. Chen, J. Xia, P. Du, H. Zheng, and L. Gan, "Multisource earth observation data for land-cover classification using random forest," *IEEE Geoscience and Remote Sensing Letters*, vol. 15, no. 5, pp. 789–793, 2018.
- [22] Y. Zhang, S. Yan, X. Jiang, L. Zhang, Z. Cai, and J. Li, "Dual graph learning affinity propagation for multimodal remote sensing image clustering," *IEEE Transactions on Geoscience and Remote Sensing*, vol. 62, pp. 1–13, 2024.
- [23] Z. Lv, H. Huang, W. Sun, T. Lei, J. A. Benediktsson, and J. Li, "Novel enhanced unet for change detection using multimodal remote sensing image," *IEEE Geoscience and Remote Sensing Letters*, vol. 20, pp. 1–5, 2023.
- [24] W. Dong, T. Zhang, J. Qu, S. Xiao, T. Zhang, and Y. Li, "Multibranch feature fusion network with self- and cross-guided attention for hyperspectral and lidar classification," *IEEE Transactions on Geoscience and Remote Sensing*, vol. 60, pp. 1–12, 2022.
- [25] X. Wu, D. Hong, and J. Chanussot, "Convolutional neural networks for multimodal remote sensing data classification," *IEEE Transactions on Geoscience and Remote Sensing*, vol. 60, pp. 1–10, 2022.
- [26] D. Li, W. Xie, Y. Li, and L. Fang, "Fedfusion: Manifold-driven federated learning for multi-satellite and multi-modality fusion," *IEEE Transactions on Geoscience and Remote Sensing*, vol. 62, pp. 1–13, 2024.
- [27] Y. Gao, M. Zhang, J. Wang, and W. Li, "Cross-scale mixing attention for multisource remote sensing data fusion and classification," *IEEE Transactions on Geoscience and Remote Sensing*, vol. 61, pp. 1–15, 2023.
- [28] L. Zhao and S. Ji, "Cnn, rmn, or vit? an evaluation of different deep learning architectures for spatio-temporal representation of sentinel time series," *IEEE Journal of Selected Topics in Applied Earth Observations and Remote Sensing*, vol. 16, pp. 44–56, 2023.
- [29] Y. Gao, X. Song, W. Li, J. Wang, J. He, X. Jiang, and Y. Feng, "Fusion classification of hsi and msi using a spatial-spectral vision transformer for wetland biodiversity estimation," *Remote Sensing*, vol. 14, no. 4, pp. 1–19, 2022.
- [30] Z. Xue, X. Tan, X. Yu, B. Liu, A. Yu, and P. Zhang, "Deep hierarchical vision transformer for hyperspectral and lidar data classification," *IEEE Transactions on Image Processing*, vol. 31, pp. 3095–3110, 2022.
- [31] Y. Feng, J. Zhu, R. Song, and X. Wang, "S2eft: Spectral-spatial-elevation fusion transformer for hyperspectral image and lidar classification," *Knowledge-Based Systems*, vol. 283, pp. 1–11, 2024.
- [32] M. Zhang, F. Gao, T. Zhang, Y. Gan, J. Dong, and H. Yu, "Attention fusion of transformer-based and scale-based method for hyperspectral and lidar joint classification," *Remote Sensing*, vol. 15, no. 3, pp. 1–15, 2023.
- [33] J. T. Smith, A. Warrington, and S. Linderman, "Simplified state space layers for sequence modeling," in *International Conference on Learning Representations*, 2023, pp. 1–13.
- [34] A. Gu and T. Dao, "Mamba: Linear-time sequence modeling with selective state spaces," *arXiv*, 2312.00752, 2024. [Online]. Available: <https://arxiv.org/abs/2312.00752>
- [35] J. Sieber, C. A. Alonso, A. Didier, M. N. Zeilinger, and A. Orvieto, "Understanding the differences in foundation models: Attention, state space models, and recurrent neural networks," *arXiv*, 2405.15731, 2024. [Online]. Available: <https://arxiv.org/abs/2405.15731>
- [36] X. Xu, W. Li, Q. Ran, Q. Du, L. Gao, and B. Zhang, "Multisource remote sensing data classification based on convolutional neural network," *IEEE Transactions on Geoscience and Remote Sensing*, vol. 56, no. 2, pp. 937–949, 2017.
- [37] M. Zhang, W. Li, Q. Du, L. Gao, and B. Zhang, "Feature extraction for classification of hyperspectral and lidar data using patch-to-patch cnn," *IEEE Transactions on Cybernetics*, vol. 50, no. 1, pp. 100–111, 2020.
- [38] S. Mohla, S. Pande, B. Banerjee, and S. Chaudhuri, "Fusatnet: Dual attention based spectrospatial multimodal fusion network for hyperspectral and lidar classification," in *2020 IEEE/CVF Conference on Computer Vision and Pattern Recognition Workshops (CVPRW)*, 2020, pp. 416–425.
- [39] S. Fang, K. Li, and Z. Li, "S²enet: Spatial-spectral cross-modal enhancement network for classification of hyperspectral and lidar data," *IEEE Geoscience and Remote Sensing Letters*, vol. 19, pp. 1–5, 2021.
- [40] Y. Hu, H. He, and L. Weng, "Hyperspectral and LiDAR data land-use classification using parallel Transformers," in *IEEE International Geoscience and Remote Sensing Symposium (IGARSS)*, 2022, pp. 703–706.
- [41] G. Zhao, Q. Ye, L. Sun, Z. Wu, C. Pan, and B. Jeon, "Joint classification of hyperspectral and LiDAR data using a hierarchical cnn and Transformer," *IEEE Transactions on Geoscience and Remote Sensing*, vol. 61, pp. 1–16, 2022.
- [42] J. Yao, B. Zhang, C. Li, D. Hong, and J. Chanussot, "Extended vision transformer (exvit) for land use and land cover classification: A multimodal deep learning framework," *IEEE Transactions on Geoscience and Remote Sensing*, vol. 61, pp. 1–15, 2023.
- [43] K. Li, D. Wang, X. Wang, G. Liu, Z. Wu, and Q. Wang, "Mixing self-attention and convolution: A unified framework for multisource remote sensing data classification," *IEEE Transactions on Geoscience and Remote Sensing*, vol. 61, pp. 1–16, 2023.
- [44] A. Gu, I. Johnson, K. Goel, K. Saab, T. Dao, A. Rudra, and C. Re, "Combining recurrent, convolutional, and continuous-time models with linear state-space layers," in *International Conference on Neural Information Processing Systems (NeurIPS)*, 2021, pp. 1–14.

- [45] A. Gu, K. Goel, and C. Ré, “Efficiently modeling long sequences with structured state spaces,” in *International Conference on Learning Representations (ICLR)*, 2022, pp. 1–13.
- [46] Y. Liu, Y. Tian, Y. Zhao, H. Yu, L. Xie, Y. Wang, Q. Ye, and Y. Liu, “Vmamba: Visual state space model,” *arXiv*, 2401.10166, 2024. [Online]. Available: <https://arxiv.org/abs/2401.10166>
- [47] X. Ma, X. Zhang, and M.-O. Pun, “Rs3mamba: Visual state space model for remote sensing image semantic segmentation,” *IEEE Geoscience and Remote Sensing Letters*, vol. 21, pp. 1–5, 2024.
- [48] K. Chen, B. Chen, C. Liu, W. Li, Z. Zou, and Z. Shi, “Rsmamba: Remote sensing image classification with state space model,” *IEEE Geoscience and Remote Sensing Letters*, vol. 21, pp. 1–5, 2024.
- [49] Q. Zhu, Y. Cai, Y. Fang, Y. Yang, C. Chen, L. Fan, and A. Nguyen, “Samba: Semantic segmentation of remotely sensed images with state space model,” *arXiv*, 2404.01705, 2024. [Online]. Available: <https://arxiv.org/abs/2404.01705>
- [50] H. Chen, J. Song, C. Han, J. Xia, and N. Yokoya, “Changemamba: Remote sensing change detection with spatiotemporal state space model,” *IEEE Transactions on Geoscience and Remote Sensing*, vol. 62, pp. 1–20, 2024.
- [51] Y. Li, Y. Luo, L. Zhang, Z. Wang, and B. Du, “Mambahi: Spatial-spectral mamba for hyperspectral image classification,” *IEEE Transactions on Geoscience and Remote Sensing*, vol. 62, pp. 1–14, 2024.
- [52] “Multimodal remote sensing benchmark datasets for land cover classification with a shared and specific feature learning model,” *ISPRS Journal of Photogrammetry and Remote Sensing*, vol. 178, pp. 68–80, 2021.
- [53] A. Okujeni, S. van der Linden, and P. Hostert, “Berlin-urban-gradient dataset 2009—an enmap preparatory flight campaign,” *GFZ Data Services*, 2016.
- [54] B. Le Saux, N. Yokoya, R. Hansch, and S. Prasad, “2018 IEEE GRSS data fusion contest: Multimodal land use classification,” *IEEE Geoscience and Remote Sensing Magazine*, vol. 6, no. 1, pp. 52–54, 2018.
- [55] Y. Gao, W. Li, M. Zhang, J. Wang, W. Sun, R. Tao, and Q. Du, “Hyperspectral and multispectral classification for coastal wetland using depthwise feature interaction network,” *IEEE Transactions on Geoscience and Remote Sensing*, vol. 60, pp. 1–15, 2021.
- [56] W. Li, Y. Gao, M. Zhang, R. Tao, and Q. Du, “Asymmetric feature fusion network for hyperspectral and sar image classification,” *IEEE Transactions on Neural Networks and Learning Systems*, vol. 34, no. 10, pp. 8057–8070, 2022.